**Engineering and Technology Journal**
**Journal homepage:** https://etj.uotechnology.edu.iq

# Effects of pumping profiles on the temperature distributions in double-end pumped solid-state lasers: A comparison study

**Hind A. Jawad, Mohammed J. AbdulRazzaq*, Khalid S. Shibib**

Laser and Optoelectronic Engineering Dept, University of Technology-Iraq, Alsina'a street, 10066 Baghdad, Iraq.
*Corresponding author Email: abdulrazzaq@uotechnology.edu.iq

## HIGHLIGHTS

- Understanding the thermal behavior of dual end-pumped solid-state lasers.
- The exponent of the beam profile has a significant effect on the temperature distributions.
- Monitoring the thermal behavior keeps the performance of the lasers before being subject to damage.
- A theoretical basis for laser cavity design of dual-end-pumped cylindrical laser rods was provided.

## ARTICLE INFO

**Handling editor:** Ivan A. Hashim
**Keywords:**
heat load; Laser rod; Pump profile; Super-Gaussian profile.

## ABSTRACT

In this work, the effects of pumping profiles on the temperature distributions in solid-state lasers pumped by laser diode from two different end faces were studied. With different pump spot radii of $0.4mm$ *and* $0.6mm$, various exponent factors were examined to evaluate the behavior of temperature distributions due to Gaussian and super-Gaussian profiles. For a Gaussian pumping (n=2), the maximum temperature difference on each rod face was calculated to be 295.5 K and 226 K, respectively, at a total pump power of 92.8 W (46.4 W per face). While at the same pumping power, the temperature decreased as the n exponent increased. A good match was obtained between the proposed model and the previous works listed in the literature.

## 1. Introduction

Understanding the induced temperature distribution over the laser active medium is important. This is due to the need for a tiny focused pump beam volume in end-pumped solid-state lasers, resulting in relatively higher pump deposition density and thus a high density of thermal loading. Such a result may lead to a regression in both beam quality and laser performance [1].

Several previous works studied the thermal model and thermal effects of solid-state lasers in different geometries [2-11]. Full temperature distribution analytical evaluations in end-pumped solid-state lasers under all profiles types were presented in Ref. [12]. A numerical investigation of thermal effects in single and double end-pumped solid-state lasers was achieved using the finite element method (FEM) for many commonly used lasers media crystals [13-14]. The FEM incorporated in LASCAD software was also used to evaluate thermal focal length and temperature distribution in a CW Nd: YAG laser rod for a double end-pumped laser media under Gaussian and super-Gaussian pumping beam profiles [15]. By taking into account thermal conductivity as a function of temperature, the analytical thermal model for the double-end laser diode pumped cylindrical laser rod was derived by solving the heat equation. Also, the temperature distribution and the thermal stresses were estimated under top-hat and Gaussian pump beam profiles by Refs [16-18]. With complicated boundary conditions utilizing COMSOL Multiphysics simulation software, the thermal model of a slab crystal was investigated. A new theoretical method to slab laser crystal (Tm: YLF) was derived for the first time by Ref. [19].

In this work, an analytical steady-state-thermal model was derived to evaluate temperature distributions in cylindrical shape solid-state lasers in dual-end-pumped geometry with Gaussian and Super-Gaussian pump beam profiles. The derived model provides a theoretical basis for laser cavity design of dual-end-pumped cylindrical laser rods.



http://doi.org/10.30684/etj.v40i2.2278
Received 11 July 2021; Accepted 18 October 2021; Available online 25 February 2022
2412-0758/University of Technology-Iraq, Baghdad, Iraq
This is an open access article under the CC BY 4.0 license http://creativecommons.org/licenses/by/4.0

## 2. Thermal modeling

The proposed 2D configuration of double-end pumping Nd: YAG laser rod is shown in Fig. 1. With an unequal pumping radius focused on the center of the laser rod from two different pumping sources, the heat was solved analytically using Kirchhoff's transformation method.

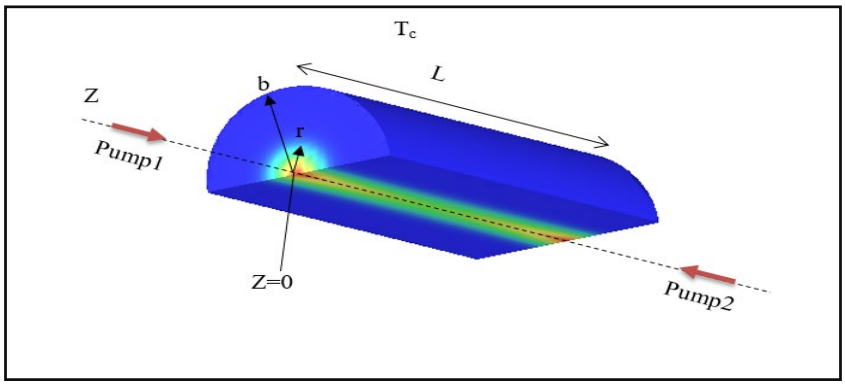


**Figure 1:** 2D pumping geometry of the rod, where the pumping sources are positioned at r = 0 and z = 0, L

The equation of steady-state heat is stated as [20]:

$$\nabla.[K(T)\nabla T(r,z)] + Q(r,z) = 0 \tag{1}$$

Where Q(r,z) denotes the heat source density, this is proportional to pump power density. The temperature-dependence thermal conductivity is denoted by K(T), which is provided by [12]:

$$K(T) = K_o \left(\frac{T}{T_o}\right)^m \tag{2}$$

where m, $K_0$, and $T_0$ are the best-fit to measured data provided by [14]. For a Super-Gaussian double-end pumping, Q(r,z) can be presented as:

$$Q_{(r,z)} = Q_1 e^{-\alpha z} e^{-2\frac{r^n}{{w_1}^n}} + Q_2 e^{-\alpha(L-z)} e^{-2\frac{r^n}{{w_2}^n}} \tag{3}$$

where $W_{1,2}$ are $1/e^2$ radii intensity profiles of the two pump beams, L is the laser's rod length, α is the pump coefficient of the absorption, and $Q_{1,2}$ are normalization constants that can be calculated using the following relation:

$$Q_{1,2} = \frac{\eta_h P_{1,2}}{V_{1,2}} \tag{4}$$

$P_{1,2}$ are the incident pump powers, the fractional heat load is denoted by $\eta_h$, and $V_{1,2}$ the volumes of pump–photon distribution in the rod which found to be:

$$V_{1,2} = \frac{2\pi\, \eta_{abs}\, {w_{1,2}}^2}{\alpha\, n\, 4^{\frac{1}{n}}} \Gamma\left(\frac{2}{n}\right) \tag{5}$$

Where Γ(a,x) denotes incomplete gamma function. Substituting $Q_{1,2}$ into Eq. (3), The laser rod's dissipated thermal power density becomes:

$$Q_{(r,z)} = \frac{n\eta\alpha}{2\pi\Gamma\left(\frac{2}{n}\right)4^{-\frac{1}{n}}} \left[\frac{1}{{w_1}^2} P_1 e^{-\alpha z} e^{-2\frac{r^n}{{w_1}^n}} + \frac{1}{{w_2}^2} P_2\, e^{-\alpha(L-z)} e^{-2\frac{r^n}{{w_2}^n}}\right] \tag{6}$$

Now the nonlinear heat equation (Equation (1)) can be translated into a linear for cylindrical rod as [1]:

$$\nabla^2 U(r,z) = -S(r,z) = \frac{\partial^2 U(r,z)}{\partial r^2} + \frac{1}{r}\frac{\partial U(r,z)}{\partial r} \tag{7}$$

Where;

$$U = \frac{K_\circ}{(m+1)T_0^m} T^{m+1} + C \tag{8}$$

C is the integration constant.

According to Figure1, the boundary conditions for establishing temperature distributions include the thermal isolation for the two-rod end faces and the entire length of the rod being in air convection. In this case, the boundary conditions take the form of :

$$-\frac{dU_{pump}}{dr}\Big|_{r=0} = 0 \tag{9}$$

$$-\frac{dU_{unpump}}{dr}\Big|_{r=b} = h\left[T_{2_{r=b}} - T_c\right] \tag{10}$$

and,

$$\frac{dT_{pump}}{dr}\Big|_{r=2w} = \frac{dT_{unpump}}{dr}\Big|_{r=2w} \tag{11}$$

Therefore, the two temperature solutions for eq. (7) in two regions (i.e. the pumped region ($0 \le r \le w$) and the unpumped region ($w < r \le b$)) are:

$$T_{pump1(r,z)} = \{A_\circ \frac{P_1}{{W_1}^2} e^{-\alpha z}[\, b^2\, 2F2\left(\frac{2}{n}, \frac{2}{n}; 1+\frac{2}{n}, 1+\frac{2}{n}; \frac{-2b^n}{{w_1}^n}\right) - r^2\, 2F2\left(\frac{2}{n}, \frac{2}{n}; 1+\frac{2}{n}, 1+\frac{2}{n}; \frac{-2r^n}{{w_1}^n}\right)] + \left(T_c + \frac{\eta_h P_1 \alpha\, e^{-\alpha z}}{4\pi b h}\right)^{m+1}\}^{\frac{1}{m+1}} \tag{12}$$

and

$$T_{pump2(r,z)} = \{A_\circ \frac{P_2}{{W_2}^2} e^{-\alpha(l-z)}[b^2\, 2F2\left(\frac{2}{n}, \frac{2}{n}; 1+\frac{2}{n}, 1+\frac{2}{n}; \frac{-2b^n}{{w_2}^n}\right) - r^2\, 2F2\left(\frac{2}{n}, \frac{2}{n}; 1+\frac{2}{n}, 1+\frac{2}{n}; \frac{-2r^n}{{w_2}^n}\right)] + \left(T_c + \frac{\eta_h P_2 \alpha\, e^{-\alpha(l-z)}}{4\pi b h}\right)^{m+1}\}^{\frac{1}{m+1}} \tag{13}$$

$$T_{pump(r,z)} = \{A_\circ[\frac{P_1}{{W_1}^2} e^{-\alpha z}\left(b^2\, 2F2\left(\frac{2}{n}, \frac{2}{n}; 1+\frac{2}{n}, 1+\frac{2}{n}; \frac{-2b^n}{{w_1}^n}\right) - r^2\, 2F2\left(\frac{2}{n}, \frac{2}{n}; 1+\frac{2}{n}, 1+\frac{2}{n}; \frac{-2r^n}{{w_1}^n}\right)\right) + \frac{P_2}{{W_2}^2} e^{-\alpha(l-z)}\left(b^2\, 2F2\left(\frac{2}{n}, \frac{2}{n}; 1+\frac{2}{n}, 1+\frac{2}{n}; \frac{-2b^n}{{w_2}^n}\right) - r^2\, 2F2\left(\frac{2}{n}, \frac{2}{n}; 1+\frac{2}{n}, 1+\frac{2}{n}; \frac{-2r^n}{{w_2}^n}\right)\right)] + \left(T_c + \frac{\eta_h \alpha}{4\pi b h}\left(P_1 e^{-\alpha z} + P_2 e^{-\alpha(l-z)}\right)^{m+1}\right\}^{\frac{1}{m+1}} \tag{14}$$

Where:

$$A_\circ = \frac{2^{\frac{2}{n}-1} n}{\Gamma\left(\frac{2}{n}\right)} \frac{\eta_h\, \alpha\, (m+1) T_0^m}{4\pi K_\circ} \tag{15}$$

and ${}_pF_q$ ( $a_1, a_2 \ldots, a_p; b_1, b_2 \ldots, b_q; x$ ) is the Generalized Hypergeometric Function, defined as in ref.[21]:

$$\mathrm{pFq}\,(\,\mathrm{a1}, \mathrm{a2}\ \ldots, \mathrm{ap};\ \mathrm{b1}, \mathrm{b2}\ \ldots, \mathrm{bq}; \mathrm{x}\,) = \sum_{k=0}^{\infty} \frac{(a_1)_k (a_2)_k \ldots (a_p)_k}{(b_1)_k (b_2)_k \ldots (b_q)_k} \frac{x^k}{k!} \tag{16}$$

Pochhammer symbol $(a)_k$ is:

$$(\mathrm{a})_\mathrm{k} = \frac{\Gamma(\mathrm{a+k})}{\Gamma(\mathrm{a})} \tag{17}$$

At the unpumped region where ($w \le r \le b$)) the temperature given by:

$$T_{unpump(r,z)} = \{\frac{\eta_h\, \alpha\, (m+1) T_0^m}{4\pi K_\circ}\left(P_1 e^{-\alpha z} + P_2 e^{-\alpha(l-z)}\right) ln(\frac{b^2}{r^2}) + \left(T_c + \frac{\eta_h \alpha}{4\pi b h}\left(P_1 e^{-\alpha z} + P_2 e^{-\alpha(l-z)}\right)^{m+1}\right\}^{\frac{1}{m+1}} \tag{18}$$

At rod surface ($r$=b) equation(18) become:

$$T_{unpump(b,z)} = T_c + \frac{\eta_h \alpha}{4\pi bh}\left(P_1 e^{-\alpha z} + P_2 e^{-\alpha(l-z)}\right) \quad (19)$$

Now, the difference of the temperatures between the center of the rod and its edge can be written as:
ΔT(r, z) = Tpump(r, z) − Tunpump(b, z)
Which is equivalent to:

$$\Delta T_{(r,z)} = \left\{\frac{2^{\frac{2}{n}-1} n}{\Gamma\left(\frac{2}{n}\right)} \frac{\eta_h\, \alpha\, (m+1) T_0^m}{4\pi K_\circ} \left[\frac{P_1}{{w_1}^2}\, e^{-\alpha z}\left(b^2\, 2F2\left(\frac{2}{n}, \frac{2}{n}; 1+\frac{2}{n}, 1+\frac{2}{n}; \frac{-2b^n}{{w_1}^n}\right) - r^2\, 2F2\left(\frac{2}{n}, \frac{2}{n}; 1+\frac{2}{n}, 1+\frac{2}{n}; \frac{-2r^n}{{w_1}^n}\right)\right) + \frac{P_2}{{w_2}^2}\, e^{-\alpha(l-z)}\left(b^2\, 2F2\left(\frac{2}{n}, \frac{2}{n}; 1+\frac{2}{n}, 1+\frac{2}{n}; \frac{-2b^n}{{w_2}^n}\right) - r^2\, 2F2\left(\frac{2}{n}, \frac{2}{n}; 1+\frac{2}{n}, 1+\frac{2}{n}; \frac{-2r^n}{{w_2}^n}\right)\right)\right]\right\}^{\frac{1}{m+1}} \quad (20)$$

## 3. Results and Discussion

To assess our proposed model, we make a comparison with an earlier analytical work presented by Refs.[16-17]. The heat loading and the radial temperature distribution had been modeled using Nd: YAG as an active medium. Table 1 lists the parameters represented in this analysis.

Under double-end Super-Gaussian pumping profile with different pump spot radii, Figure 2 shows the influence of $n^{th}$ order on the behavior of the generated heat load. It can be seen that as the $n^{th}$ exponent increases, Q(r,z) is decreased on both rod end faces, and the shape of the pump profile becomes more flattened. It was also observed that the heat deposition is increased as the spot radius decreased, as indicated in Figure 2 (a and b). Under the Gaussian pump profile where n=2 and for the same laser parameters, the obtained results perfectly match a previous work presented by Ref. [17].

Figure 3 (a and b) depict the temperature distribution between the rod center and the rod surface. With different pump spot radii $(i.e\ w_1 = 0.4, w_2 = 0.6mm)$. For the same laser parameters listed by Ref.[17], the maximum temperature of 295.5 K and 225.9 K were obtained on both rod end faces. For n much greater than two, which tend to a top-hat profile, the temperatures gradient between the center and surface of the laser rod were shown in figures 3c,d. The obtained results are perfectly matched for the same parameters listed by Ref. [16].

**Table 1:** Input Laser Parameters

| **Parameters** | **[17]** | **[16]** |
|---|---|---|
| Heat loading rate (η) | 0.25 | 0.24 |
| Rod radius (b) | 1.5 mm | 1.25 mm |
| Rod length (L) | 10 mm | 5 mm |
| Absorption coefficient (α) | 350 $m^{-1}$ | 350 $m^{-1}$ |
| Thermal conductivity (ko) | 13 $W.m^{-1}.K^{-1}$ | 15.09 $W.m^{-1}.K^{-1}$ |
| Reference temperature (To) | 227 K | 164.17 k |
| Heat sink temperature (Tc) | 300 K | 300 k |
| power coefficient for thermal conductivity (m) | -0.56 | -0.75 |
| Thermal conductance (h) | 0.02 $W.mm^{-2}.K^{-1}$ | 0.02 $W.mm^{-2}.K^{-1}$ |
| Pump spot radii (W1,2) | 0.4,0.6 mm | 0.4,0.6 mm |

The various effects of the beam spot radius and the exponent factor on the steady-state axial temperature distribution of the gain medium are shown in Figure 4 (a-d). It was observed that along the rod axis, the temperature decreased exponentially due to the incident power's exponentially absorbed.

Also, Figure 5a-e shows the contour mapping of the temperature distribution on each face of the super-Gaussian pumped region for different n's factors, namely (2, 8,16, and 32) respectively, which indicate that the maximum temperature in laser media is reduced as the $n^{th}$ exponent increased.

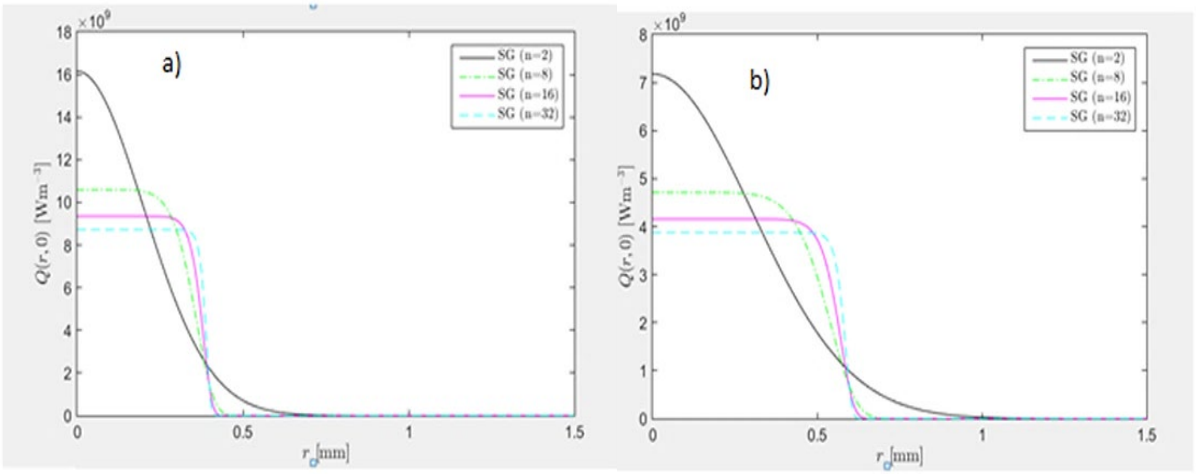


**Figure 2:** Heat load for double-end-super-Gaussian pumping, (a) for w=0.4mm and (b) for w=0.6mm

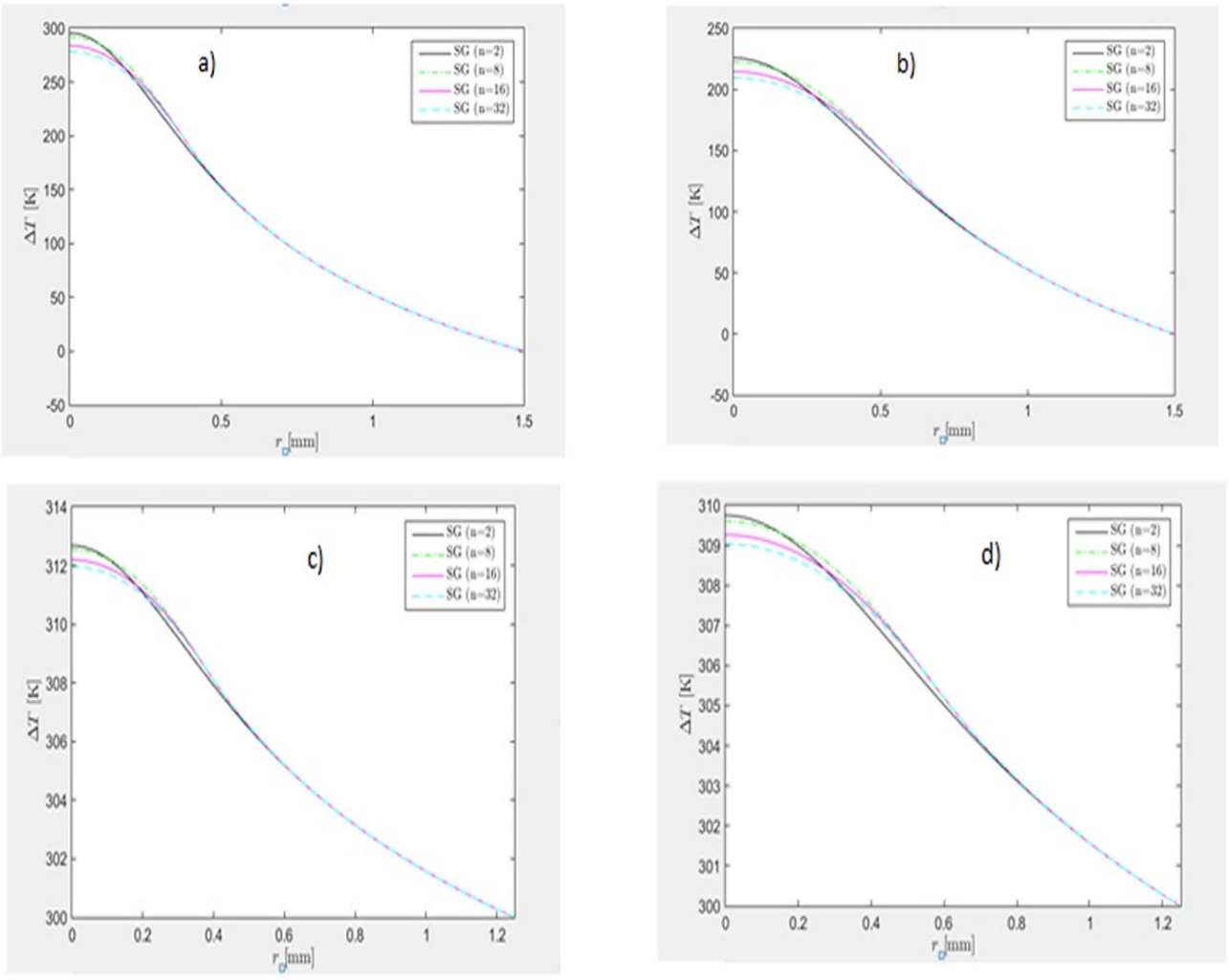


**Figure 3:** Gaussian at (a) w=0.4mm, (b) w=0.6mm, and Top-hat at (c) w=0.4mm, and (d) w=0.6mm

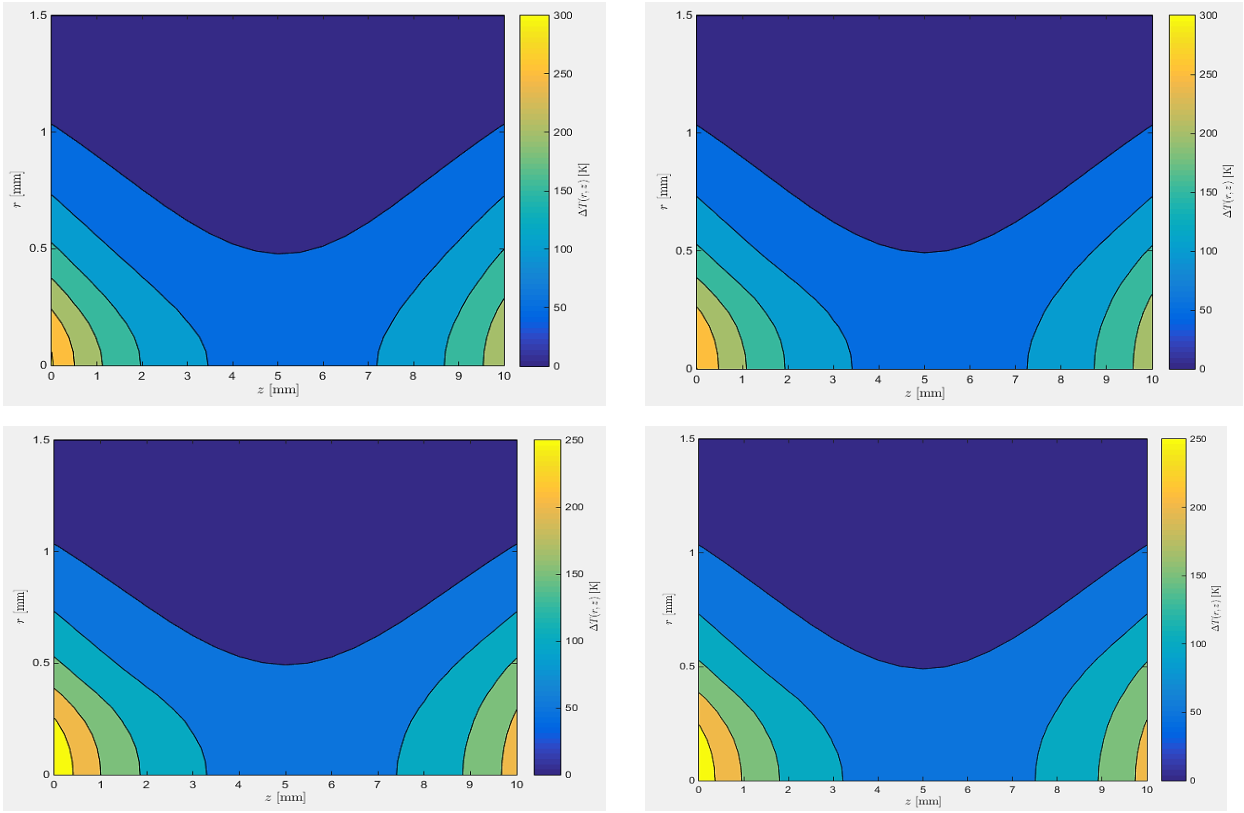

**Figure 4:** Temperature distribution of super-Gaussian along the medium at (a) n=2, (b) n=8, (c) n=16, and (d)n=32

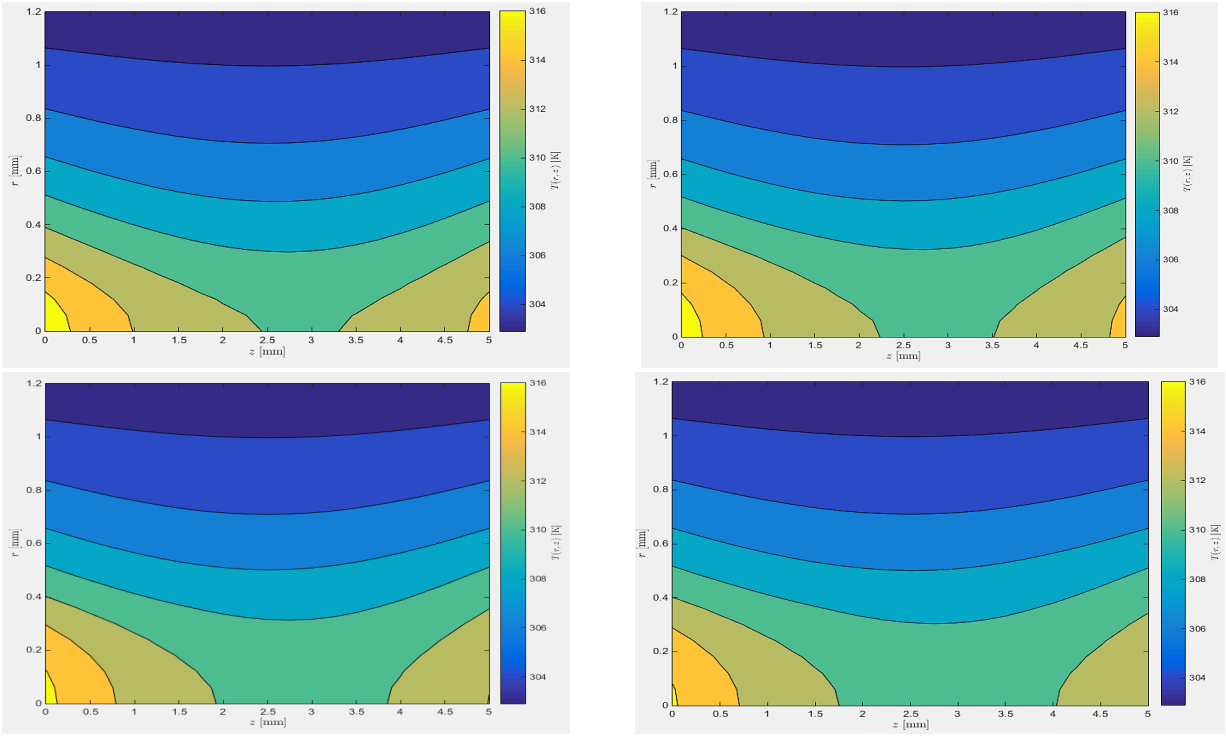

**Figure 5:** Contour mapping of temperature distribution in laser rod for (a) n=2, (b) n=8, (c) n=16, and (d) n=32

## 4. Conclusions

In conclusion, the effects of pumping profiles on the thermal effects in double-end-pumped solid-state lasers were modeled analytically using Kirchhoff's integral transform method. By taking into account different pump radii focused on the end faces of the laser rod with various $n^{th}$ exponent factors, the behavior of the temperature distributions was obtained, and a good matching was obtained with previous works listed in the literature. Furthermore, the results show that as the exponent of the Gaussian pumping beam profile increased, the maximum temperature difference in the laser rod decreased exponentially since the beam became flatter than the Gaussian profile.

**Author contribution**
All authors contributed equally to this work.
**Funding**
This research received no specific grant from any funding agency in the public, commercial, or not-for-profit sectors.
**Data availability statement**
The data that support the findings of this study are available on request from the corresponding author.
**Conflicts of interest**
The authors declare that there is no conflict of interest.

## References

**[1]** W. A. Clarkson, Thermal effects and their mitigation in end-pumped solid-state lasers, J. Phys. D: Appl. Phys., 34 (2001) 2381–2395. http://dx.doi.org/10.1088/0022-3727/34/16/302

**[2]** M. J. Abdul-razzak, Simulation of Thermal Effects in Totally and Partially Pumped Solid-State Laser Rod with Side-Pumping Structure, Eng. Technol. J., 32 (2014) 608–616.

**[3]** M. J. Abdul Razzaq, A. K. Abass, W. Y. Nassir, Thermal Lensing Reduction in Conventional and Composite Nd:YAG Laser Rod, Eng. Technol. J., 34 (2016) 2031–2035. http://dx.doi.org/10.30684/etj.34.11A.9

**[4]** B. A. Usievich, V. A. Sychugov, F. Pigeon, A. Tishchenko, Analytical treatment of the thermal problem in axially pumped solid-state lasers, IEEE J. Quantum Electron., 37 (2001) 1210–1214. http://dx.doi.org/10.1109/3.945327

**[5]** K. S. Shibib, MA Munshid, NE Alattar, Thermal and stress analysis in Nd: YAG laser rod with different double end pumping methods, Therm. Sci., 15 (2011) 399-407. http://dx.doi.org/10.2298/TSCI101201004S

**[6]** K. S. Shibib, M.M Tahir, H.I Qatta, Analytical model of transient temperature and thermal stress in continuous wave double-end-pumped laser rod: Thermal stress minimization study, Pramana., 79 (2012) 287-297. https://doi.org/10.1007/s12043-012-0295-4

**[7]** K. S. Shibib, M.A Munshid, K.A Hubiter, Analytical model of transient thermal effect on convectional cooled end-pumped laser rod, Pramana., 81(2013) 603-615. https://doi.org/10.1007/s12043-013-0600-x

**[8]** F. Kalantarifard, H. Nadgaran, P. Elahi, The analytical and numerical investigation of thermo-optic effects in double-end-pumped solid state lasers, Int. J. Phys. Sci., 4 (2009) 385–389.

**[9]** Y. Kwon, Thermal modeling of solid state lasers with super-Gaussian pumping profiles, Opt. Eng., 42 (2003) 1787. http://dx.doi.org/10.1117/1.1572499

**[10]** M. Mojahedi , H. Shekoohinejad, Thermal Stress Analysis of a Continuous and Pulsed End-Pumped Nd:YAG Rod Crystal Using Non-Classic Conduction Heat Transfer Theory, Braz. J. Phys., 48 (2018) 46–60. http://dx.doi.org/10.1007/s13538-017-0538-4

**[11]** J. Liu, X. Chen, Y. Yu, C. Wu, F. Bai, G. Jin, Analytical solution of the thermal effects in a high-power slab Tm:YLF laser with dual-end pumping, Phys. Rev. A., 93 (2016) 1–7. http://dx.doi.org/10.1103/PhysRevA.93.013854

**[12]** L. Cini , J. I. Mackenzie, Analytical thermal model for end-pumped solid-state lasers, Appl. Phys. B . Opt., 123 (2017) 273. http://dx.doi.org/10.1007/s00340-017-6848-y

**[13]** M. Sayem El-Daher, Finite element analysis of thermal effects in diode end-pumped solid-state lasers, Adv. Opt. Technol., 2017 (2017) 9256053. http://dx.doi.org/10.1155/2017/9256053

**[14]** R. M. El-Agmy , N. Al-Hosiny, Thermal analysis and experimental study of end-pumped Nd: YLF laser at 1053 nm, Photonic. Sens., 7 (2017) 329–335. http://dx.doi.org/10.1007/s13320-017-0412-6

**[15]** H. Alrawi, M. J. AbdulRazzaq, A. K. Abass, Numerical thermal model of diode double-end-pumped solid state lasers, Int. J. Nanoelectron. Mater., 11 (2018) 473–480.

**[16]** M. J. AbdulRazzaq, A. Z. Mohammed, A. K. Abass, . K. S. Shibib, A new approach to evaluate temperature distribution and stress fracture within solid state lasers, Opt. Quant. Electron., 51 (2019) 294. http://dx.doi.org/10.1007/s11082-019-2012-8

**[17]** M. J. AbdulRazzaq, K. S. Shibib, S. I. Younis, Temperature distribution and stress analysis of end pumped lasers under Gaussian pump profile, Opt. Quant. Electron., 52 (2020) 379. https://doi.org/10.1007/s11082-020-02499-y

**[18]** M. J. Abdulrazzaq , K. A. Hubeatir, Analysis of Thermal Effects within Cylindrical Shape Solid-State Laser Rod, 1002 (2020) 264–272. http://dx.doi.org/10.4028/www.scientific.net/MSF.1002.264

**[19]** C. Xinyu, L. Jingliang, W. Chunting, W. Ruiming, J. Guangyong, Thermal Effects Analysis of High-Power Slab Tm:YLF Laser with Dual-End-Pumped Based on COMSOL Multiphysics, Integr. Ferroelectr., 210 (2020) 197–205. http://dx.doi.org/10.1080/10584587.2020.1728823

**[20]** W. Xie, Thermal and optical properties of diode side-pumped solid state laser rods, Opt. Laser. Technol., 32 (2000) 193–198. http://dx.doi.org/10.1016/S0030-3992(00)00042-6

**[21]** S. I. El-Soubhy, Notes on Generalized Hypergeometric and Confluent Hypergeometric Functions, Int. J. Math. Anal. Appl., 2 (2015) 47–61.